A Flexible Reduced Graphene Oxide Field-Effect Transistor for Ultrasensitive Strain Sensing

*Tran Quang Trung, Nguyen Thanh Tien, Doil Kim, Mi Jang, Ok Ja Yoon, and Nae-Eung Lee**

A new kind of flexible strain sensor based on a reduced graphene oxide field-effect transistor (rGO FET) with ultrasensitivity, stability, and repeatability for the detection of tensile and compressive strains is demonstrated. The novelty of the rGO FET strain sensor is the incorporation of a rGO channel as a sensing layer in which the electrical resistance can be greatly modified upon application of an extremely low level of strain resulting in an intrinsically amplified sensing signal. The rGO FET device is ultrasensitive to extremely low strain levels, as low as 0.02%. Due to weak coupling between adjacent nanosheets, therefore, upon applying small levels of strain into the rGO thin film, a modulation of the internanosheet resistance (R_{inter}) is expected, inducing a large change in the transconductance of the rGO FET. Using a simple printing and self-assembly process, the facile fabrication of an rGO FET array over a large area is also demonstrated. In addition, the device can detect small and rapid physical movements of the human body.

1. Introduction

Recently, various flexible pressure, strain, thermal, and optical sensors have been extensively studied for personal health monitoring, electronic skins, robot sensors, and other human-machine interface requiring mechanical conformality.[1–13] For high responsivity to external stimuli, many sensors have been fabricated by using a number of nano-scale sensing materials including nanowire,[5–9] carbon nanotubes,[14,15] graphene[10,16–20] and hybrid nanocomposite[11–13,21,22] on various stretchable or flexible substrates. Among those, many strain sensors using a resistor structure where changes in conductance or resistance of piezoresistive sensing layer under strain are monitored have been developed.[6,7,10,13–15,17–19,21,22] While most of them have been still used for detection of a large strain range of about a few to tens of percentages,[14,15,19,21,22] ultrasensitive strain sensor having the detection limit less than 0.1% has been rarely reported. Furthermore, transport properties in the piezoresistive sensing layer upon strain for understanding of sensing mechanism are not easily extractable. Development of ultrasensitive strain sensors having the capability of detecting extremely low strain levels in electronic skins, robot sensors or other human-machine interfaces is of great interest.

Among various strain sensing materials, graphene is a fascinating carbon nanostructure and has received strong interest due to its exceptional electrical, mechanical and optical properties.[23–25] There have been some recent reports demonstrating that the strain can dramatically modify the electronic and optical properties of graphene.[20,26–29] Moreover, under strain, the band gap of graphene can be opened because of the breaking of the sublattice symmetry of the two carbon sublattices of graphene.[29,30] Based on these features, graphene is a promising candidate as a strain sensing material. There have been only a few approaches to assemble a strain sensor from a single sheet of graphene utilizing chemical vapor deposition (CVD),[17–19] epitaxial growth,[10,19] or mechanical exfoliation.[20] However, graphene-based devices used in ultrasensitive strain sensors still have some limitations. For example, modification of the electrical resistance is required under an applied tensile strain but the device cannot detect small levels of strain (the minimum strain that can detected in the graphene-based resistor device was less 2.47% [17] and the sensing mechanism was not elucidated in detail. In addition, ultrasensitive strain sensing can be possible by observing shifts of the Raman spectrum[20] but this approach requires costly equipment, making it uneconomical for real-life applications.

Another interesting form of strain sensing layer is a networked film of graphene nanosheets. Graphene nanosheets, which are manufactured by the chemical exfoliation of graphite, are often called reduced graphene oxide (rGO) nanosheets.[31–33] Studies of electronic conduction in the rGO network have shown that the conduction is attributed to two main components: (i) intra-nanosheet resistance (R_{intra}) controlled by

Prof. N.-E. Lee
School of Advanced Materials Science & Engineering
SKKU Advanced Institute of Nanotechnology (SAINT)
and, Samsung Advanced Institute for
Health Sciences & Technology (SAIHST)
Sungkyunkwan University (SKKU)
Suwon, Kyunggi-do, 440–746, Korea
E-mail: nelee@skku.edu
Mr. T. Q. Trung, Dr. N. T. Tien, Mr. D. Kim, Dr. O. J. Yoon
School of Advanced Materials Science & Engineering
Sungkyunkwan University (SKKU)
Suwon, Kyunggi-do, 440–746, Korea
Ms. M. Jang
SKKU Advanced Institute of Nanotechnology (SAINT)
Sungkyunkwan University (SKKU)
Suwon, Kyunggi-do, 440–746, Korea

DOI: 10.1002/adfm.201301845

disorders arising from residual oxygen functional groups, intrinsic structural defects, and defects generated during the fabrication process of single rGO nanosheets, and (ii) inter-nanosheet resistance (R_{inter}) affected by coupling between adjacent nanosheets.[31,32,34–36] Under the strain mode, the resistance (R_{inter} and R_{intra}) or conductance of network rGO films is expected to be strongly modulated because the strain modes can possibly affect disorders and defects inside the nanosheets as well as coupling between adjacent nanosheets. Based on these aspects, networked rGO thin films can be used to fabricate ultrasensitive strain sensors.

Herein, we report a new kind of flexible ultrasensitive strain sensor based on a reduced graphene oxide field-effect transistor (rGO FET) using a simple solution processable fabrication process. The novelty of the rGO FET strain sensor is the incorporation of an rGO channel as the sensing layer in which the electrical resistance can be greatly modified upon application of an extremely low level of strain resulting. Since signal from strain sensors based on filed-effect transistor (FET) platform can be also amplified and various electrical parameters can be readily extracted,[2,3,36,37] integration of strain sensing layer as a channel into the field-effect transistor (FET) structure is a practical approach for better understanding of sensing mechanism in sensing layer as well as for development of ultrasensitive strain sensing devices with flexibility, stability, and repeatability and expected to provide significant contributions to not only strain sensing research fields but also real-life applications. The rGO FET device was ultrasensitive to extremely low strain levels as low as 0.02%. Furthermore, the devices show high stability and repeatability in addition to fast response and relaxation. Due to weak coupling between adjacent nanosheets, therefore, upon applying small levels of strain into a rGO thin film, a strong modulation of R_{inter} can be expected, inducing a large change of the transconductance of the rGO FET. The device also demonstrated good performance in terms of its sensing characteristics including sensitivity, stability, reproducibility, and the response and relaxation times after 10 000 bending cycles at tensile strains of 0.2 and 0.35%. In addition, the capability of measuring the distribution of the normalized current (I_{DS}/I_{DS0}) from each device in the rGO FET array under strain was demonstrated. It was also demonstrated that the device could detect small and rapid physical movements of the human body.

2. Results and Discussion

The rGO FET array was fabricated on a flexible and transparent polyethersulfone (PES) substrate. The details of fabrication process are explained in the Experimental Section. Using this simple fabrication process, facile fabrication of sixteen rGO FETs on the total area of 193 mm^2 was demonstrated. The schematic of the device array is shown in **Figure 1**a. Using the simple fabrication process described in the Experimental Section, an average yield of 87.5% was obtained. As an example, the transfer characteristics of the sixteen devices in a fabricated rGO FET array are shown in Supporting Figure S1. Figure 1b shows the photographs of the device array under tensile and compressive strain loads. And electric responses of a flexible rGO FET in the array to mechanical strains were obtained by recording the normalized current change (Figure 1c).

To study the electrical behaviors of the rGO FET in response to mechanical strain, the source-drain current (I_{DS}) and transfer characteristics of the devices by a sweeping gate bias (V_G) were measured upon application of various strains at room temperature. The dependence of the rGO FET performance on different applied strain modes (tensile and compressive) was evaluated for two different strain levels, extremely small (0.02 to 0.08%) and small strains (0.1 to 0.35%). The method of strain calculation is explained in Supporting Figure S2. **Figures 2**a and b show the transfer characteristics of the rGO FETs under tensile and compressive strains of 0.1 to 0.35%, respectively. The I_{DS}–V_G characteristics are ambipolar. That is, both electron and hole currents can be induced by the V_G. The typical response of I_{DS} to tensile and compressive strains in the device results in opposite trends in which an increase of the I_{DS} upon application of compressive strain and a decrease of the I_{DS} upon application of tensile strain occurred. The minimum source-drain current ($I_{DS,\ min}$) values at the charge neutrality point (CNP) in the transfer curves shown in Figures 2a and b are presented as a function of the measured tensile and compressive strains in Figure 2c. And the differences of rGO FET when used as a strain sensor instead of an element in flexible electronic device were discussed in detail in Supporting Information.

To explain the strain sensing mechanism of the rGO FET, the strain-induced modulation of the resistance in the rGO channel may be the key to understanding the effects of tensile and compressive strains on the I_{DS} modulation of the devices. It is known that the inter-nanosheet resistance (R_{inter}) of a network rGO film is controlled by modulation of charge-hopping transport and carrier mobility by coupling at nanosheet junctions,[34–36] which may be expected to change greatly upon an applied strain. Tensile strain may reduce coupling at nanosheet junctions, leading to an increase of the resistance of the network rGO film and thus, a decrease of the I_{DS} (Figure 2a and c). The I_{DS} increased as the compressive strain increased (Figure 2b and c), which results from the decrease of resistance in the rGO channel, presumably due to reinforcement of coupling at the nanosheet junctions under compressive strain. To further demonstrate that the I_{DS} modulation of rGO FET by tensile and compressive strains is primarily controlled by resistance change of the rGO channel induced by change in the coupling between adjacent nanosheets, resistance modulation of the rGO film under tensile and compressive strains was additionally obtained in a resistor configuration with no gate dielectric layer. The resistance modulation of the rGO resistor presented in Supporting Figure S3a shows a tendency similar to that of the FET, which indicates that the I_{DS} modulation in Figure 2 was primarily caused by the resistance change in the rGO channel. And, a comparison of the responsivity from resistor and FET structures presented in Supporting Figure S3b indicates that the responsivity of FET sensor to strain can be reinforced by controlling V_G due to signal amplification in FET structure.

However, recent reports have demonstrated that the change of the performances of organic field-effect transistors (OFET) upon applied strain is not only due to the modulation of the channel resistance and capacitance of the dielectric layer, but also from the contribution of changing surface energy and

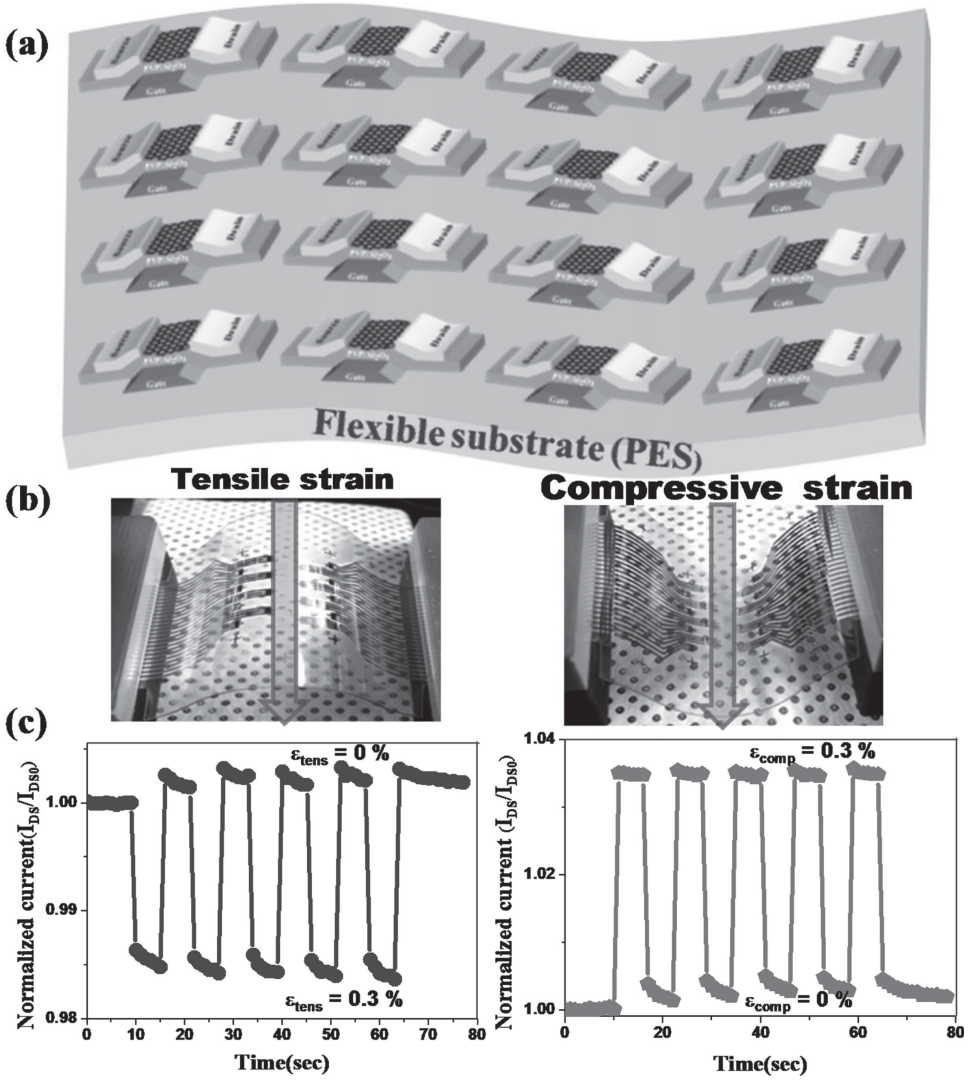

Figure 1. a) The rGO FET was fabricated on a flexible polyethersulfone (PES) substrate. By self-assembly of GO nanosheets and reduction, the device array can be fabricated by the formation of a GO channel pattern on the locally-coated SAM pattern. b) The photographs of the device array under tensile and compressive strain loads. c) Electrical responses of a flexible rGO FET in the array to the tensile and compressive strains obtained by recording the normalized current change.

surface dipole of polymer dielectric which results from rearrangement of the polymer chains.[38] In our device structure, for the adsorption of GO nanosheets on a hybrid organic/inorganic (poly-4-vinylphenol (PVP)/Al_2O_3) dielectric, a poly(diallyldimethylammonium chloride) (PDDA) self-assembled monolayer (SAM) was formed on Al_2O_3. With straining at the interface between the SAM and R-GO channel, however, it is difficult to rearrange polymer chains of PDDA due to a few single-layers of PDDA, resulting in no change of the surface energy and surface dipoles. To demonstrate that the PDDA SAMs do not affect the strain sensing behavior of the rGO FET, we examined two additional types of rGO FETs: (i) a rGO FET with a (3-aminopropyl)triethoxysilane (APTES) SAM and (ii) a rGO FET without a SAM. In case of the device without the SAM, the Al_2O_3 surface was treated in nitrogen plasma before attachment of GO nanosheets. The transfer characteristics of the devices were measured under tensile and compressive strains ranging from 0.1 to 0.35%. The strain sensing behaviors of the devices showed the same tendencies as those of the rGO FET with PDDA SAMS (see Supporting Figures S4 and S5). The results indicate that the strain sensing mechanism of rGO FETs is mainly attributed to the contribution of resistance variations in strained rGO channels.

As aforementioned, the resistance change in strained rGO channel is primarily induced by the change in R_{inter} rather than the change in R_{intra}. To prove that the resistance change is mainly attributed to the change in R_{inter}, we also examined strain sensing behaviors of the FET structure with a single graphene active layer (graphene FET) that was synthesized by CVD. In this case, the size of graphene is larger than the channel length with no R_{inter}. For comparison of the strain sensing characteristics of graphene FET with that of rGO FET, the transfer characteristics of graphene FET was measured under tensile strain and the resistance change of graphene was also

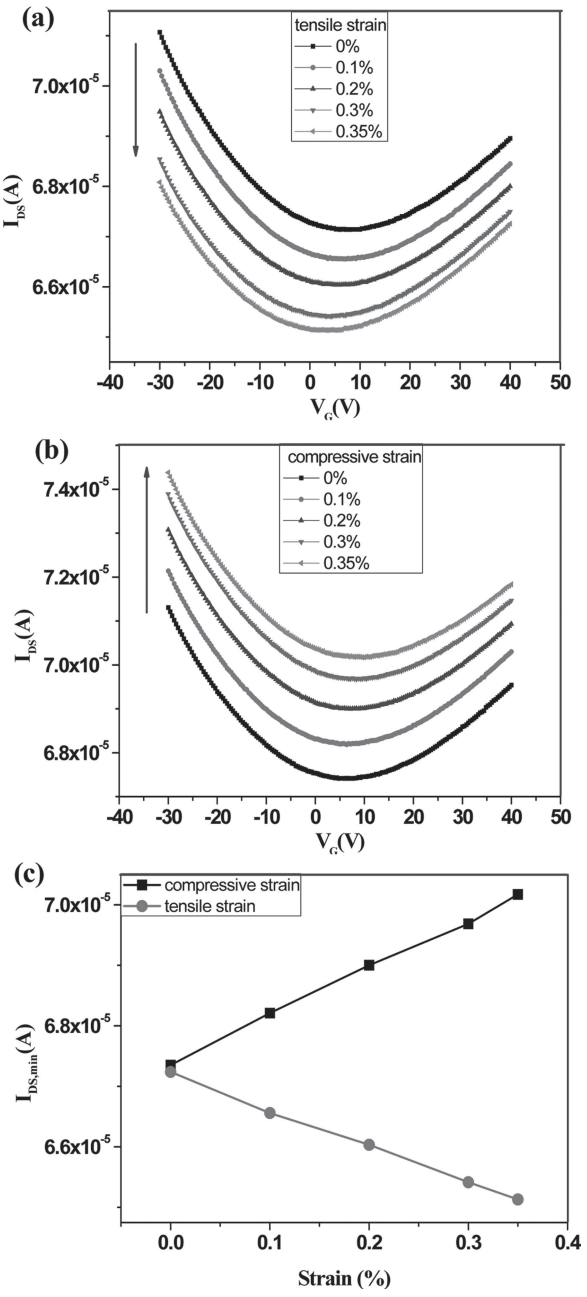

Figure 2. The transfer characteristics of the rGO FET at different a) tensile and b) compressive strains. During the measurements, the source-drain voltage (V_{DS}) was fixed at 3 V. c) The modulation of the minimum source-drain current ($I_{DS,min}$) under applied tensile and compressive strains.

measured under compressive strain (Supporting Figure S6). The resistance changes of rGO and graphene under compressive strain were calculated from I_{DS} and V_{DS}. In this case, V_G was not applied on the rGO and graphene FET to make sure that modulation of the I_{DS} or channel resistance upon compressive strain is mainly contributed by active layers without interference from capacitance of gate dielectric layer. The data in Supporting Figure S6 show that the I_{DS} and channel resistance of graphene FET were nearly unchanged under tensile and compressive strains, respectively. These results confirm that the

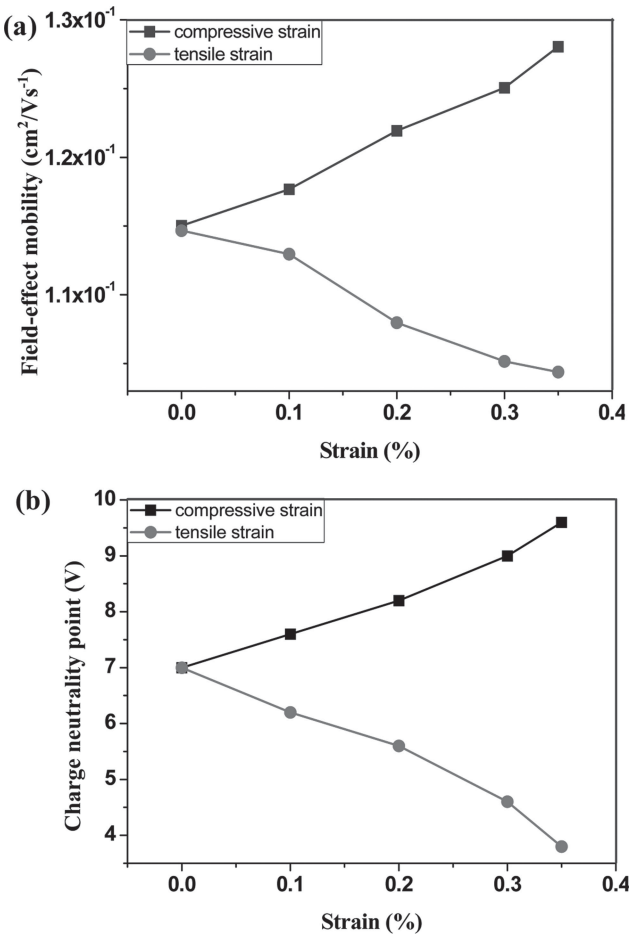

Figure 3. a) The hole field-effect mobility, μ_{FE}, as a function of the tensile and compressive strains. b) The variation of the charge neutrality point (CNP) under applied tensile and compressive strains.

I_{DS} in strained rGO FET is mainly modulated by the variation in R_{inter} of rGO channel.

To elucidate the effects of the tensile and compressive strains on the channel resistance variations in the rGO FET as well as the strain sensing mechanism of the device, the field-effect mobility, μ_{FE}, and CNP were extracted from the transfer characteristics of the rGO FET under various tensile and compressive strains. **Figure 3**a presents the variation of μ_{FE} under applied tensile and compressive strains. In the rGO FET, the electron mobility, μ_e, is smaller than the hole mobility, μ_h.[34] Thus, the μ_{FE} of a rGO FET can be presented as the hole field-effect mobility (the detailed calculation method of field-effect hole mobility is presented in Supporting Figure S7). To understand the modulation of μ_{FE} under strain, Mattthiessen's rule is normally used for the overall FET mobility. Therefore, $1/\mu_{FE}$ can be written as the sum of $1/\mu_{int}$ and $1/\mu_{ext}$, as shown in Equation (1).[39]

$$\frac{1}{\mu_{FE}} = \frac{1}{\mu_{int}} + \sum_{i,ext} \frac{1}{\mu_{i,ext}} \quad (1)$$

$$\sum_{i,ext} \frac{1}{\mu_{i,ext}} = \frac{1}{\mu_{PB}} + \frac{1}{\mu_{CI}} + \frac{1}{\mu_{SR}} + \frac{1}{\mu_{SPP}} \quad (2)$$

Here, μ_{int} represents the carrier mobility limited by intrinsic scattering such as the longitudinal acoustic phonon scattering, carrier-carrier scattering, and rGO defects and μ_{ext} is the mobility limited by extrinsic scattering.[31,39] In Equation (2), μ_{PB} is the mobility limited by scattering at the potential barrier (PB) between adjacent nanosheets[31] and μ_{CI}, μ_{SR}, and μ_{SPP} are the mobilities limited by scattering from the Coulomb impurities (CI), the surface roughness (SR), and the dielectric surface polar phonon (SPP) in the nanosheets, respectively.[39] Upon straining of rGO FETs, the variation of the μ_{ext} of the device is expected to mainly cause a change of the μ_{FE} due to negligible changes of the intrinsic scatterings. Therefore, the contribution from changes of the μ_{ext} of the rGO channel should be investigated in order to understand the modulation of μ_{FE} under applied strain.

In order to understand the observed modulation direction of the μ_{FE} variation in the rGO FET under applied tensile and compressive strains, the effects of the PB change on the μ_{ext} of the rGO channel were explored. As is well known, the magnitude of the PB between individual components of the nanoparticulates and nanowires which affects hopping transport or the mobility of carriers is dependent on coupling between individual components.[40–42] Similarly, the condition of coupling between adjacent two-dimensional rGO nanosheets inside the channel affects the degree of overlapping and the gap between rGO nanosheets at nanosheet junctions and, in turn, determines the junction area and the magnitude of the PB, respectively. The junction area and the magnitude of PB are expected to affect carrier hopping transport and the μ_{PB} of the rGO FET, respectively, resulting in the modulation of μ_{ext} and R_{inter}. Under tensile strain, decreased junction area and larger gap in the network rGO thin film may limit carrier transport and decrease μ_{ext} due to enhanced scattering, respectively, (Figure 3a) and, in turn, increase R_{inter} (Supporting Figure S3) in the rGO channel. In contrast, the increase of the μ_{ext} (Figure 3a) and the decrease of the R_{inter} upon the application of compressive strain are caused by decreased height of PB leading to reduced carrier scattering and enhanced hopping transport due to increased junction area, respectively, at nanosheet junctions.

Figure 3b shows the CNP shifts of the rGO FET as a function of tensile and compressive strains in opposite directions. There are many different factors that govern the position of the CNP in rGO or graphene FETs including (i) doping inside the rGO or graphene,[43,44] (ii) rGO or graphene defects,[45] (iii) a dielectric layer (residual dipoles inside dielectric, gate capacitance, and morphology of the surface),[39,46] (iv) dipolar adsorbates (water and oxygen molecules) on the top surface of rGO or graphene and the rGO/dielectric or graphene/dielectric interface,[47,48] and (v) charge injection from rGO or graphene to the dielectric interface.[39] Under applied strain, the capacitance of the gate dielectric layer based on factor (iii) is affected.[49] The gate capacitance decreases under compressive strain and increases under tensile strain (see Supporting Figure S8).[49] The change of the capacitance is attributed to the change of the thickness of dielectric layers induced by the Poisson effect.[49] Therefore, modulation of the CNP under applied tensile and compressive strains can be expected by the variation of the capacitance in the gate dielectric layer.

To further investigate the strain sensing performance of the rGO FET, the sensing characteristics during repetitive straining conditions were studied by measuring the time-dependent I_{DS} under various applied tensile and compressive strains. **Figures 4**a and b show the time-dependence of the normalized current, I_{DS}/I_{DS0} (I_{DS}: current under applied strain, I_{DS0}: current without applied strain), under extremely small levels of applied tensile and compressive strains ranging from 0.02 to 0.08%, respectively. The results in Figure 4a and b indicate that the devices possess ultrahigh strain sensitivity with the capability of detecting even the smallest tensile and compressive strains of 0.02%. In addition, the time-dependence of the I_{DS}/I_{DS0} of the rGO FET upon small applied tensile and compressive strains ranging from 0.1 to 0.3% was also measured (Figures 4c and d). In this case, the time of applying and releasing the strain was 1 s, and the response and relaxation times of the device also corresponded to 1 s, which demonstrate the capability of the rGO FET device to respond and relax very quickly to dynamic tensile and compressive straining.

For reliable evaluation of the strain responsiveness in the rGO FET, the stability and repeatability of the sensing characteristics under dynamic straining were evaluated under ambient conditions. In response to 50 applied tensile and compressive strain cycles, the time-dependent I_{DS} was monitored where the results shown in Figures 4e and f correspond to tensile and compressive cyclic straining, respectively. In this case, the tensile and compressive strains were kept constant at 0.3%, the interval time for the applied and released strain was 2 s for each cycle, and the time to reach tensile and compressive strains of 0.3% was 1 s. Besides the slight variation of the sensitivity and base current, the rGO FETs demonstrated good repeatability of the current response and relaxation time during the tensile and compressive straining cycles. Based on these results, the rGO FETs after repetitive mechanical deformation were judged to be highly stable with repeatable responses to dynamic tensile and compressive strains. Additionally, the effects of oxygen, moisture, or other molecules at ambient condition on the response of our device are negligible under different tensile and compressive strains.

For further evaluation of the reliability of rGO FETs after repetitive mechanical deformations, the sensing capability, repeatability, response time, and relaxation time of the device were evaluated after cyclic bending of the devices (see Supporting Figure S9 for details of the electrical performance of cyclically bent devices). The time-dependence of the normalized current (I_{DS}/I_{DS0}) of the rGO FET upon applied tensile and compressive strains of 0.3% was monitored after the device was subjected to10, 100, 1000, and 10 000 bending cycles at strains of 0.2% (see Supporting Figures S9a and S9b) and 0.35% (see Supporting Figures S9c and S9d). The stable responses of I_{DS}/I_{DS0} to tensile and compressive strains after cyclic bending after cyclic bending indicate good repeatability of the sensing performances including the current response, response time, and relaxation time.

To demonstrate the potential application of the rGO FET strain sensor in personal health monitoring, "smart" surgical gloves, or human-machine interfaces, we examined the sensing capability of the device to movements of the human body. For this purpose, a PES substrate with a rGO FET was

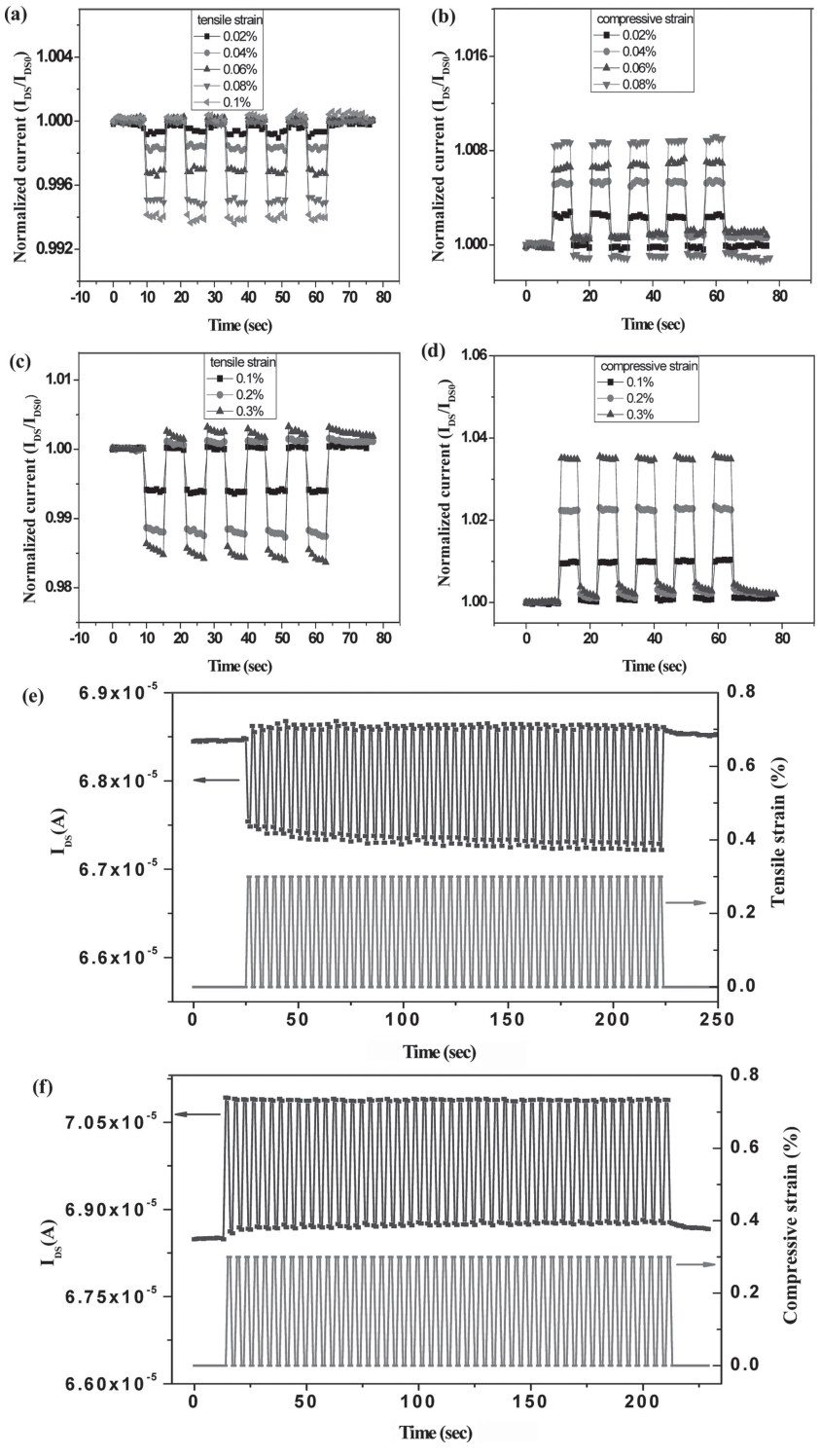

Figure 4. The time-dependence of the normalized current, I_{DS}/I_{DS0} (I_{DS}: current under applied strain, I_{DS0}: current without applied strain) upon extremely small applied a) tensile and b) compressive strains ranging from 0.02 to 0.08% was monitored. The time-dependence of I_{DS}/I_{DS0} upon small levels of applied (c) tensile and (d) compressive strains ranging from 0.1 to 0.3% was also monitored. The time-dependence of I_{DS} under applied cyclic e) tensile and f) compressive strains was monitored. Fifty cycles of tensile and compressive strain were applied to the R-GO FETs and the dynamic electrical responses were recorded. During monitoring of the I_{DS}, the V_g and V_{DS} were fixed at 5 and 3 V, respectively.

attached onto a thumb. The I_{DS} response was recorded at a V_{DS} of 3 V and a V_G of 5 V for bending motions of the finger (see the inserts in **Figures 5**a and b). The I_{DS} rapidly decreased and increased, which is consistent with the responsiveness of the device to tensile and compressive strains upon bending-up (Figure 5a) and bending-down (Figure 5b) thumb motions, respectively. In addition, the I_{DS} recovered to the original current after each bending and release motion cycle.

To demonstrate the sensing capability of the rGO FET in a device array under strain, we measured the normalized current (I_{DS}/I_{DS0}) of the sixteen rGO FETs in the device array under a compressive strain of 0.35% at the centre of the device array (Figure 5c). Figure 5d shows an example of the distribution of the normalized current (I_{DS}/I_{DS0}) obtained from each device in the array. The normalized current values (I_{DS}/I_{DS0}) of the devices at the edge positions (columns 1 and 4) are smaller than the devices at the centre positions (columns 2 and 3) because the strains at columns 2 and 3 are expected to be higher than those at columns 1 and 4. When strain is applied to the rGO FET array, the strain magnitude at the centre is higher than at the edge. Therefore, there is a strain distribution profile from the centre to the edge of the rGO FET array. Based on these features, the rGO FET array offers a great deal of promise for electronic skin applications.

3. Conclusions

We demonstrated ultrasensitive strain sensing of a flexible rGO FET device and a rGO FET array prepared by a simple fabrication process. The rGO FET strain sensor showed ultrasensitivity at extremely low straining modes, high reliability, and fast response and relaxation characteristics. The ultrasensitivity of the rGO FETs to strain variation is primarily attributed to channel resistance variations in the rGO channel due to weak coupling between adjacent nanosheets. Upon introduction of a small strain into a rGO thin channel, modulation of the inter-nanosheet resistance (R_{inter}) leads to a change of the output current of the rGO FET. Besides the ultrasensitivity, excellent reproducibility, and fast response and relaxation times were also demonstrated in the rGO FETs under repetitive strain sensing. Also, the rGO FETs showed excellent reliability under repetitive mechanical deformation up to 10 000 bending cycles at tensile strains of

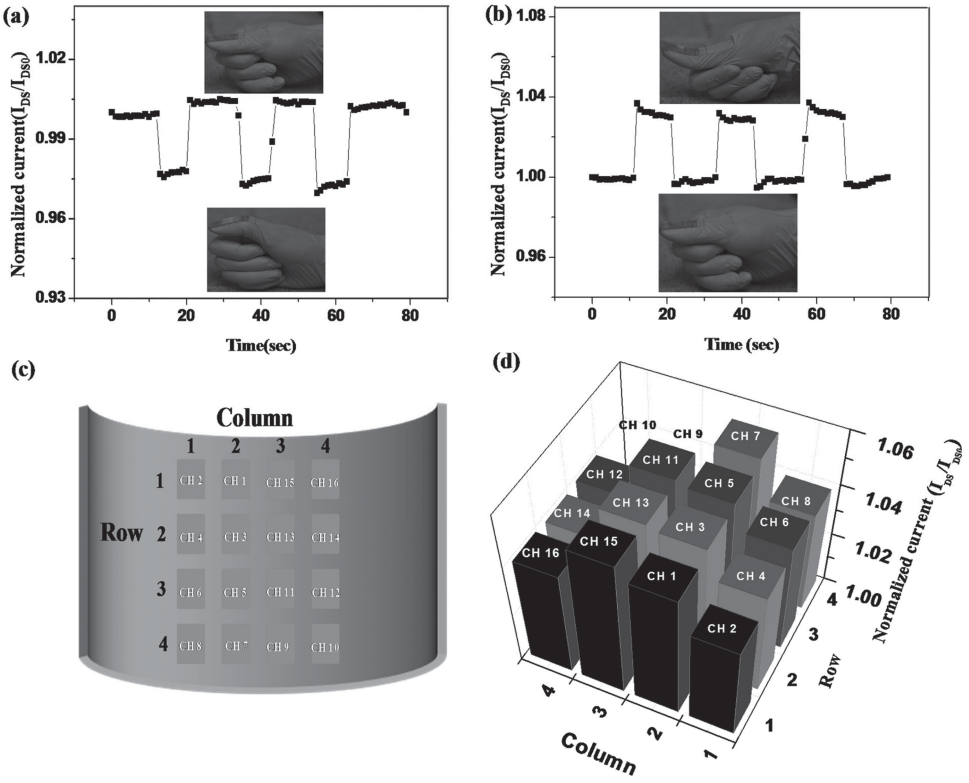

Figure 5. Responses of the rGO FET to motions of a finger were measured: a) the time-dependence of I_{DS} under motion of the finger corresponding to applied tensile strain and b) the time-dependence of I_{DS} under motion of the finger corresponding to applied compressive strain. During monitoring of the I_{DS}, the V_g and V_{DS} were fixed at 5 and 3 V, respectively. c) The positions of each device in the rGO FET array under a compressive strain of 0.35% are indicated as a channel. d) The distribution of the normalized current (I_{DS}/I_{DS0}) from each device corresponding to the position of each device in the array is shown.

0.2% and 0.35% without significant degradation of their electrical characteristics. The features of the rGO FET array offer a great deal of promise for flexible applications in personal health monitoring, electronic skin, "smart" surgical gloves, or human-machine interfaces.

4. Experimental Section

The rGO FET array devices were fabricated on transparent and flexible polyethersulfone (PES) substrates. The gate electrode (Ni) was deposited onto a PES substrate through a shadow mask by e-beam evaporation. The gate dielectric layer was formed by spin-coating a cross-linkable PVP (poly-4-vinyl phenol) solution and subsequent annealing in a nitrogen environment at 200 °C for 1 h. A graphene oxide (GO) networked film was first fabricated from chemically exfoliated graphene oxide nanosheets from graphite flakes using a modified Hummer's method.[31,32] To form a thin continuous networked GO film, a 20 nm thick Al_2O_3 buffer layer was deposited by atomic layer deposition (ALD) on the gate dielectric layer (PVP) and was modified by poly(diallyldimethylammonium chloride) (PDDA) self-assembled monolayers (SAMs) to enhance the adsorption of GO nanosheets. The fabrication process of the rGO FET array is described as follows. First, the surface of Al_2O_3 corresponding to a rGO channel of each device was selectively modified by printing a PDDA pattern using a syringe pump (see Supporting Figure S11). The GO solution in water (0.2 mg/mL) was selectively absorbed on the PDDA-modified substrates of the Al_2O_3 layer. The networked GO film was reduced to rGO by exposure to hydrazine hydrate vapor at 40 °C for 18 h. Then, the Au (50 nm)/Cr (5 nm) source (S) and drain (D) electrodes were thermally evaporated on rGO thin films through a shadow mask. To improve the performance of rGO FETs and eliminate interactions of the rGO channel with oxygen and water adsorption, which can cause electrical instability, the FET devices were encapsulated by a tetratetracontane (TTC, $CH_3(CH_2)_{42}CH_3$) layer after annealing the whole device at 150 °C for 3 h under a high vacuum of 10^{-5} Torr. The highly hydrophobic TTC layer minimizes adsorption of polar solvents such as water vapor and is therefore, a good capping material for the encapsulation of the rGO FET array.

Supporting Information

Supporting Information is available from the Wiley Online Library or from the author.

Acknowledgements

This research was supported by the Basic Science Research Program (Grant No. 2010–0015035 and 2013R1A2A1A01015232) and the WCU Program (Grant No. R32–2008–000–10124–0) through the National Research Foundation of Korea (NRF) funded by the Ministry of Education, Science and Technology.

Received: May 29, 2013
Revised: June 19, 2013
Published online: July 22, 2013

[1] T. Someya, Y. Kato, T. Sekitani, S. Iba, Y. Noguchi, Y. Murase, H. Kawaguchi, T. Sakurai, *Proc. Natl. Acad. Sci. USA* **2005**, *102*, 12321.
[2] S. C. B. Mannsfeld, B. C. K. Tee, R. M. Stoltenberg, C. V. H. H. Chen, S. Barman, B. V. O. Muir, A. N. Sokolov, C. Reese, Z. Bao, *Nature Mater.* **2010**, *9*, 859.
[3] T. Q. Trung, N. T. Tien, Y. G. Seol, N.-E. Lee, *Org. Electron.* **2012**, *13*, 533.
[4] G. Schwartz, B. C.-K. Tee, J. Mei, A. L. Appleton, D. H. Kim, H. Wang, Z. Bao, *Nat. Commun.* **2013** DOI: 10.1038/ncomms2832
[5] K. Takei, T. Takahashi, J. C. Ho, H. Ko, A. G. Gillies, P. Leu, R. S. Fearing, A. Javey, *Nature Mater.* **2010**, *9*, 821.
[6] C. Pang, G. Y. Lee, T. Kim, S. M. Kim, H. N. Kim, S. H. Ahn, K. Y. Suh, *Nature Mater.* **2012**, *11*, 795.
[7] R. He, P. Yang, *Nature Nanotechnol.* **2006**, *1*, 42.
[8] W. Wu, X. Wen, Z. L. Wang, *Science* **2013**, *340*, 952.
[9] S. Bai, W.i Wu, Y. Qin, N. Cui, D. J. Bayerl, X. Wang, *Adv. Funct. Mater.* **2011**, *21*, 4464.
[10] J. Zhao, C. He, R. Yang, Z. Shi, M. Cheng, W. Yang, G. Xie, D. Wang, D. Shi, G. Zhang, *Appl. Phys. Lett.* **2012**, *101*, 063112.
[11] A. T. Sepúlveda, F. Fachin, R. Guzmán de Villoria, B. L. Wardle, J. C. Viana, A. J. Pontes, L. A. Rocha, *Procedia Engin.* **2011**, *25*, 140.
[12] Y. Yang, Z.-H. Lin, T. Hou, F. Zhang, Z. L. Wang, *Nano Res.* **2012**, *12*, 888.
[13] N. Liu, G. Fang, J. Wan, H. Zhou, H. Long, X. Zhao, *J. Mater. Chem.* **2011**, *21*, 18962.
[14] D. J. Lipomi, M. Vosgueritchian, B. C. K. Tee, S. L. Hellstrom, J. A. Lee, C. H. Fox, Z. Bao, *Nature Nanotechnol.* **2011**, *6*, 788.
[15] T. Yamada, Y. Hayamizu, Y. Yamamoto, Y. Yomogida, A. Najafabadi, D. N. Futaba, K. Hata, *Nature Nanotechnol.* **2011**, *6*, 296.
[16] X. Lee, T. Yang, X. Li, R. Zhang, M. Zhu, H. Zhang, D. Xie, J. Wei, M. Zhong, K. Wang, D. Wu, Z. Li, H. Zhu, *Appl. Phys. Lett.* **2013**, *102*, 163117.
[17] X. W. Fu, Z. M. Liao, J. X. Zhou, Y. B. Zhou, H. C. Wu, R. Zhang, G. Jing, J. Xu, X. Wu, W. Guo, D. Yu, *Appl. Phys. Lett.* **2011**, *99*, 213107.
[18] S.-H. Bae, Y. Lee, B. K. Sharma, H.-J. Lee, J.-H. Kim, J.-H. Ahn, *Carbon* **2013**, *51*, 236.
[19] Y. Wang, R. Yang, Z. Shi, L. Zhang, D. Shi, E. Wang, G. Zhang, *ACS Nano* **2011**, *5* 3645.
[20] T. Yu, Z. Ni, C. Du, Y. You, Y. Wang, Z. Shen, *J. Phys. Chem. C* **2008**, *112*, 12602.
[21] X. Xiao, L. Yuan, J. Zhong, T. Ding, Y. Liu, Z. Cai Y. Rong, H. Han, J. Zhou, Z. L. Wang, *Adv. Mater.* **2011**, *23*, 5440.
[22] S. Yun, X. Niu, Z. Yu, W. Hu, P. Brochu, Q. Pei, *Adv. Mater.* **2012**, *24*, 1321.
[23] H. Chen, M. B. Muller, K. J. Gilmore, G. G. Wallace, D. Li, *Adv. Mater.* **2008**, *20*, 3557.
[24] P. Avouris, *Nano Lett.* **2010**, *10*, 4285.
[25] D. Li, *Science* **2008**, *320*, 1170.
[26] S. M. Choi, S. H. Jhi, Y. W. Son, *Phys. Rev.B* **2010**, *81*, 081407.
[27] K. Xue, Z. Xu, *Appl. Phys. Lett.* **2010**, *96*, 063103.
[28] T. M. G. Mohiuddin, A. Lombardo, R. R. Nair, A. Bonetti, G. Savini, R. Jalil, N. Bonini, D. M. Basko, C. Galiotis, N. Marzari, K. S. Novoselov, A. K. Geim, A. C. Ferrari, *Phys. Rev.B* **2009**, *79*, 205433.
[29] Z. H. Ni, T. Yu, Y. H. Lu, Y. Y. Wang, Y. P. Feng, Z. X. She, *ACS Nano* **2008**, *2*, 2301.
[30] S. M. Choi, S. H. Jhi, Y. W. Son, *Nano Lett.* **2010**, *10*, 3486.
[31] G. Eda, M. Chhowalla, *Adv. Mater.* **2010**, *22*, 2392.
[32] O. C. Compton, S. B. T. Nguyen, *Small* **2010**, *6*, 711.
[33] X. Huang, Z. Yin, S. Wu, X. Qi, Q. He, Q. Zhang, Q. Yan, F. Boey, H. Zhang, *Small* **2011**, *7*, 1876.
[34] T. Kobayashi, N. Kimura, J. Chi, S. Hirata, D. Hobara, *Small* **2010**, *6*, 1210.
[35] G. Eda, M. Chhowalla, *Nano Lett.* **2009**, *9*, 814.
[36] T. Q. Trung, N. T. Tien, D. Kim, J. H. Jung, O. J. Yoon, N. E. Lee, *Adv. Mater.* **2012**, *24*, 5254.
[37] J. Yu, X. Yu, L. Zhang, H. Zeng, *Sens. Actuat. B* **2012**, *173*, 133.
[38] A. N. Sokolov, Y. Cao, O. B. Johnson, Z. Bao, *Adv. Funct. Mater.* **2012**, *22*, 175.
[39] Z. Liu, A. A. Bol, W. Haensch, *Nano Lett.* **2011**, *11*, 523–528.
[40] E. S. Snow, J. P. Novak, P. M. Campbell, D. Park, *Appl. Phys. Lett.* **2003**, *82*, 2145.
[41] S. Kumar, J. Y. Murthy, M. A. Alam, *Phys. Rev. Lett.* **2005**, *95*, 066802.
[42] Q. Wan, E. N. Dattoli, W. Y. Fung, W. Guo, Y. Chen, X. Pan, W. Lu, *Nano Lett.* **2006**, *6*, 2909.
[43] J. T. Han, B. J. Kim, B. G. Kim, J. S. Kim, B. H. Jeong, S. Y. Jeong, H. J. Jeong, J. H. Cho, G. W, Lee, *ACS Nano* **2011**, *5*, 8884.
[44] J. Yang, J. W. Kim, H. S. Shin, *Adv. Mater.* **2012**, *24*, 2299.
[45] I. Childres, L. A. Jauregui, M. Foxe, J. Tian, R. Jalilian, I. Jovanovic, Y. P. Chen, *Appl. Phys. Lett.* **2010**, *97*, 173109.
[46] Z. Yan, Z. Sun, W. Lu, J. Yao, Y. Zhu, J. M. Tour, *ACS Nano* **2011**, *5*, 1535.
[47] K. T. Nguyen, D. Abdula, C. L. Tsai, M. Shim, *ACS Nano* **2011**, *5*, 5273.
[48] T. Lohmann, K. V. Klitzing, J. H. Smet, *Nano Lett.* **2009**, *9*, 1973.
[49] T. Sekitani, Y. Kato, S. Iba, H. Shinaoka, T. Someya, *Appl. Phys. Lett.* **2005**, *86*, 073511.